

An In Situ Formed Surface Coating Layer Enabling LiCoO₂ with Stable 4.6 V High-Voltage Cycle Performances

Yi Wang, Qinghua Zhang, Zhi-Chen Xue, Lufeng Yang, Junyang Wang, Fanqi Meng, Qinghao Li, Hongyi Pan, Jie-Nan Zhang, Zheng Jiang, Wanli Yang, Xiqian Yu,* Lin Gu,* and Hong Li*

The development of high-voltage LiCoO₂ is essential for achieving lithium-ion batteries with high volumetric energy density, however, it faces a great deal of challenges owing to the materials, structure and interfacial instability issues. In this work, a strategy is developed, through heat annealing a precoated surface layer to in situ form a high-voltage-stable surface coating layer, which is demonstrated to be highly effective to improve the high-voltage performance of LiCoO₂. It is discovered that LiCoO₂ reacts with Li_{1.5}Al_{0.5}Ti_{1.5}(PO₄)₃ (LATP) at 700 °C to form exclusively spinel phases in addition to Li₃PO₄, which are structurally coherent to the layered lattice of LiCoO₂. The heat annealing of the precoated thin layer of LATP enables the formation of a high-quality surface layer. Spinel phases possess high-voltage-stable structures with much weaker oxidizing ability of lattice oxygen than layered structure. In addition, the Li₃PO₄ is a good lithium-ion conductor with excellent chemical stability at high voltages. All these benefits contribute to the construction of a uniform and conformal high-voltage-stable surface layer with favorable lithium conducting kinetics at the LiCoO₂ surface. The modified LiCoO₂ shows excellent 4.6 V high-voltage cycle performance at both room temperature and 45 °C. The thermal stability is greatly enhanced as well.

profound impact on our daily life.^[1] LiCoO₂ has the highest material density among all commercially available cathode materials due to the perfect layered crystal structure with a cubic close-packed oxygen-anion framework, and therefore the LiCoO₂ battery has the highest volumetric energy density, which is one of the most critical performance specifications for portable electronic LIBs.^[2] Meanwhile, it is also because of the perfect layered structure, the transition metal (TM) slab of layered lattice has strong tendency to glide after removal of lithium ions at high voltages, leading to the unfavorable phase transitions (e.g., O3 to H1-3 at ≈4.5 V vs Li/Li⁺) and the resultant particle fracture.^[3] This is even severer for LiCoO₂ than other types of layered cathodes (e.g., high nickel oxides) wherein the pre-existence or the electrochemical-driven migration of transition metal cations in lithium layer (cation mixing) can more or less inhibit the glide of the layered lattice.^[4] Besides the intrinsic bulk structure instability

1. Introduction

The discovery of layered LiCoO₂ cathode by Prof. J. B Goodenough in 1980 led to the invention and successful commercialization of lithium-ion batteries (LIBs), which have been making a

nature, the surface instability issues become more pronounced at high voltages.^[5] On the one hand, the recent research reveals that the lattice oxygen of LiCoO₂ is activated after removal of half lithium (Li_{0.5}CoO₂, 4.2 V vs Li/Li⁺) and becomes highly catalytic to oxidize carbonate electrolytes that are inherently not


Dr. Y. Wang, Dr. Q. Zhang, Z.-C. Xue, Dr. L. Yang, J. Wang, F. Meng, Dr. Q. Li, H. Pan, Dr. J.-N. Zhang, Prof. X. Yu, Prof. L. Gu, Prof. H. Li
Beijing Advanced Innovation Center for Materials Genome Engineering
Key Laboratory for Renewable Energy
Beijing Key Laboratory for New Energy Materials and Devices
Institute of Physics
Chinese Academy of Sciences
Beijing 100190, China
E-mail: xyu@iphy.ac.cn; lgu@iphy.ac.cn; hli@iphy.ac.cn

Dr. Y. Wang, J. Wang, Prof. X. Yu, Prof. H. Li
Center of Materials Science and Optoelectronics Engineering
University of Chinese Academy of Sciences
Beijing 100049, China

Prof. Z. Jiang
Shanghai Synchrotron Radiation Facility
Shanghai Institute of Applied Physics
Chinese Academy of Sciences
Shanghai 201204, China

Dr. W. Yang
Advanced Light Source
Lawrence Berkeley National Laboratory
Berkeley, CA 94720, USA

Prof. X. Yu, Prof. H. Li
Yangtze River Delta Physics Research Center Co., Ltd.,
Liyang 213300, China

 The ORCID identification number(s) for the author(s) of this article can be found under <https://doi.org/10.1002/aenm.202001413>.

DOI: 10.1002/aenm.202001413

stable at voltages above 4.2 V (vs Li/Li⁺).^[6] On the other hand, the electrolyte decomposition products, cathode electrolyte interphase (CEI), have also been found unstable at high voltages and involved in a dynamic evolution of dissolution-deposition over charge–discharge cycles.^[7] As a result, the surface of LiCoO₂ cannot be passivated and unceasing electrode/electrolyte side reactions occur, leading to an increasing rise of cell resistances, and eventually, failure of batteries. At present, the commercial LiCoO₂ LIBs are restricted by an upper charging cut-off voltage of 4.4 V (graphite as anode) that allows the utilization of only around 0.62 mol lithium. To further improve the energy-density of LiCoO₂ battery, it requires further elevation of the charging voltage, in particular to voltages of above 4.6 V (vs Li/Li⁺), which can make around 25% increment (vs 4.4 V) for capacity.

Surface modifications have been demonstrated as an effective strategy to improve the cycle stability of LiCoO₂ at high voltages.^[8] Various surface doping and coating strategies using different types of doping elements and coating materials, and through different synthesis methods have been reported previously.^[9] For example, a recent study reported a Li–Al–F surface-modified LiCoO₂ showing excellent cycling performances at 4.6 V. It was revealed that the surface doping layer can restrain the harmful irreversible phase transition of LiCoO₂ at voltage above 4.55 V.^[10] More recently, our work on trace Ti–Mg–Al codoping for LiCoO₂ also greatly improved its cycle performance at 4.6 V, it was found that the surface doping of Ti and its surface segregation stabilized the lattice oxygen of LiCoO₂ and contributed to its enhanced high-voltage cycle stability.^[11] While various studies have shown promising high-voltage cycle performances of LiCoO₂, the working mechanisms for their modification strategies are different.^[12] Overall, an ideal surface modification strategy should enable the construction of a high-voltage chemically/electrochemically stable and low-resistant surface layer for LiCoO₂. Besides, the surface layer should be uniform and conformal for homogenizing the lithium flux during the charge–discharge process. This is particularly important for LiCoO₂ when cycled high-voltages, as the structure is easy to collapse at highly delithiated state and the local variation of lithium content due to the inhomogeneous lithium de-/intercalation may accelerate this process.

In this work, we have developed a method to construct a high-voltage-stable layer with appropriate lithium conducting property at the LiCoO₂ surface. First, the nanosized Li_{1.5}Al_{0.5}Ti_{1.5}(PO₄)₃ (LATP) fine particles are coated on micro-sized LiCoO₂ particles by a mechanical mixing method. Then, through high-temperature annealing, LATP reacts with LiCoO₂, converting the surface of LiCoO₂ to spinel Co₃O₄ phase while forming other spinel phases (CoAl₂O₄ and Co₂TiO₄ alike) and Li₃PO₄ simultaneously. Spinel oxide is known to have much weaker oxidizing ability at high voltages than layered oxide, and the oxygen activity has been considered as the root cause of the surface instability. The in situ formed spinel phases can thus inhibit the electrode/electrolyte side reactions and stabilize the LiCoO₂ surface. LATP and newly formed Li₃PO₄ are both lithium ionic conductors with high chemical stability at high voltages. Moreover, the well-controlled mechanical mixing and the subsequent heat annealing processes ensure the

engineering of a thin, uniform, and conformal surface layer. All these factors contribute to the substantially improved cycle stability of LiCoO₂ at high voltages. The LiCoO₂, surface modified with 2 wt% LATP through the above-mentioned method, exhibits superior 4.6 V cycle and rate performances at both room temperature and 45 °C. The improved thermal stability has also been revealed.

2. Results and Discussions

Figure 1a schematically illustrates the interface engineering for LiCoO₂ using a commercial product (denoted as bare-LCO) and nano-LATP (Figures S1 and S2, Supporting Information) as the precursor materials by a solid-state reaction method. Briefly, bare-LCO was mechanically mixed with LATP (~2 wt%) thoroughly by mechanical mixing, forming LATP-coated LCO sample (LATP@LCO), which was then annealed at various temperatures to form a uniform protective coating for LCO with strong chemical bonding. Specifically, the sample annealed at 700 °C is denoted as LATP@LCO-700. X-ray diffraction analysis (XRD) was performed to examine the phase purity of the LiCoO₂ after surface treatment (Figure S3, Supporting Information), and all XRD patterns show similar profiles of a typical LiCoO₂ without notable impurity phases, indicating the well-preserved bulk structure of LiCoO₂ during the annealing process. The morphology evolutions of the bare-LCO and the LATP@LCO samples annealed at various temperatures were investigated by scanning electron microscope (SEM), shown in Figure 1b–g. It can be found that the relatively smooth surface of bare-LCO is homogeneously coated with a rough layer of uniform small particles after mechanical mixing with LATP. The surface then becomes smooth and compact as the annealing temperatures increase from room temperature to 550 °C, and it evolves into newly grown grains with larger particle sizes at 700 °C. However, the observed grains gradually aggregate together as the temperature further increases to above 800 °C. Thus, notwithstanding that the bulk structure remains unchanged during the annealing process, the observed morphological changes imply that chemical reactions between LiCoO₂ and LATP may occur at the surface of the LATP@LCO sample.

On the question of what impacts of the annealing temperatures have on the structural and electrochemical properties of the LATP@LCO samples, we performed preliminary electrochemical cycling tests for the samples that annealed at various temperatures. The results of the electrochemical cycling in Figure S4 in the Supporting Information reveal that the LATP@LCO samples annealed at higher temperature (≥700 °C) exhibit a significantly enhanced capacity with the LATP@LCO-700 presents the best cycling stability, which strongly suggests that the surface structure might have been changed under high-temperature annealing. Thus, X-ray photoelectron spectroscopy (XPS) was carried out to study the possible surface structural evolution mechanism. Interestingly, the XPS spectra in Figure 1h show that the position of Ti 2p peaks of the obtained LATP@LCO sample after ball milling is close to that of the doped Ti in the bare-LCO rather than that for the LATP, indicating the decomposition of LATP on the LiCoO₂ surface after their mechanically mixing. Further, the position of Ti 2p peaks for the annealed

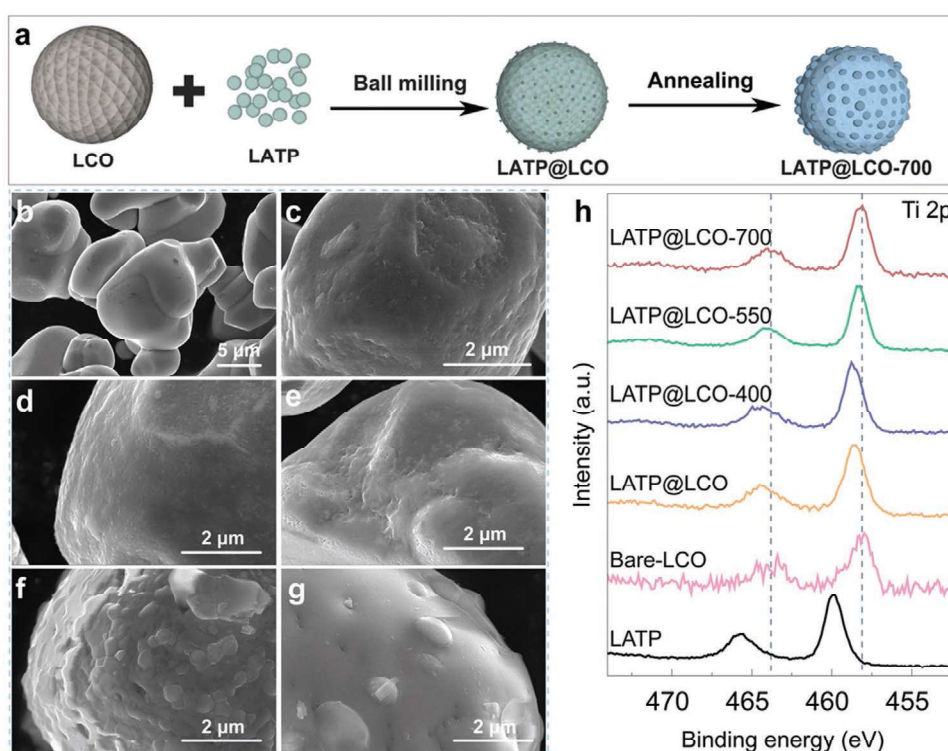


Figure 1. a) Schematic illustrations of the surface engineering of LCO. SEM images of b) bare-LCO and c) LATP@LCO without heat treatment. The LATP@LCO sample annealed at various temperatures: d) 400 °C, e) 550 °C, f) 700 °C, and g) 800 °C. h) XPS Ti 2p spectra for the precursor samples and the LATP@LCO samples annealed at various temperatures.

LATP@LCO samples progressively shift toward that of bare-LCO with the increase of the annealing temperatures, and well overlapped at the temperature of 700 °C, which imply that a new surface structure that has similar Ti chemical environment to that of the bare-LCO was constructed (note that the P signal can be observed on P 2p XPS spectra for all LATP pre-coated samples; Figure S5, Supporting Information). Thus, it is speculated that the surface coating layer should have a strong binding state with the bulk for the LATP@LCO-700 sample. Furthermore, the energy-dispersive X-ray spectroscopy (EDS) mapping analysis on LATP@LCO-700 (Figure S6, Supporting Information) reveals that the Co, P, Ti, and Al elements are homogeneously distributed on the surface of the sample, demonstrating that a uniform coating layer has been constructed on LiCoO₂ surface. Since the LATP@LCO-700 shows the best electrochemical performances, detailed characterizations were carried out to elucidate the working mechanisms.

The surface structure of the as-prepared LATP@LCO-700 sample was investigated by high-angle annular dark-field scanning transmission electron microscope (HAADF-STEM) imaging and elemental mapping based on electron energy loss spectra (EELS) (Figure 2a–h; another representative region is displayed in Figure S7 in the Supporting Information). Figure 2a displays the overall morphology of the probed particle, which shows a relatively neat surface. Detailed separated crystalline structures between the bulk and the surface of the sample were uncovered by the high-resolution HAADF images (Figure 2b) captured in the selected region as highlighted in Figure 2a. With a detailed analysis on their local lattice fringe,

it was surprising to find that, while the bulk structure remains a pristine layered structure with an interplane spacing of 0.47 nm that corresponding to the lattice plane (003) of LiCoO₂ (Figure 2c), the surface layer structure exhibits identifiable spinel structural feature with a thickness of around 10–20 nm, as indicated by the spinel structure model (Figure 2d). Thus, these findings suggest that the pristine (rhombohedral phase) LATP coating layer transformed into a spinel-like phase after the high-temperature sintering (note that unreacted LATP particle still can be found on the surface of LiCoO₂, probably due to poor contact or scattered giant LATP particles, and thus the poor reaction kinetics; see Figure S8 in the Supporting Information). Further, EELS mapping analysis on the coating layer in Figure 2e–h reveals a concentration-gradient Ti distribution in the surface region. Thus, it can be deduced that the newly formed surface Ti-rich spinel-like phase can be a result of the chemical reaction between the bulk (LiCoO₂) and the surface (LATP) at 700 °C.

In order to understand the reaction mechanism between LiCoO₂ and LATP, XRD experiments were performed to investigate the reaction products of the LiCoO₂ and LATP powder mixtures heat-treated at different temperatures for 1 h (mass ratio of around 67:23). It can be found that progressive reactions between LiCoO₂ and LATP occur with the increase of the temperatures (Figure 2i). Detailed Rietveld refinement results are shown in Figure S9 and Tables S1 and S2 in the Supporting Information. It is very interesting to note that only at the temperature of 700 °C of our interest, except for the olivine Li₃PO₄ phase, all other phases are spinel (Co₃O₄, CoAl₂O₄, and

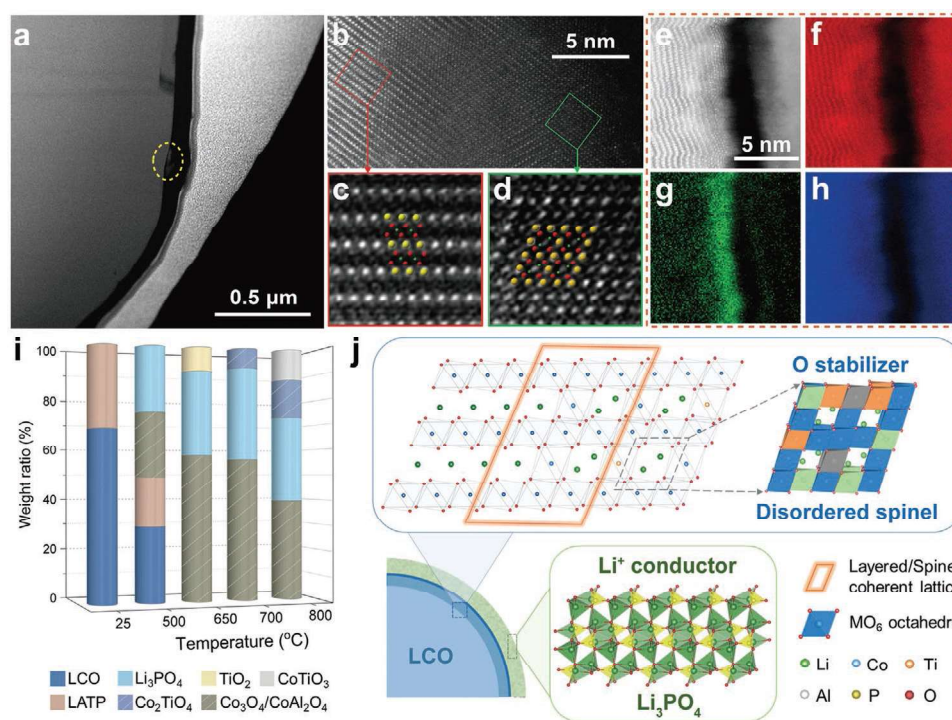


Figure 2. a) Low-magnification STEM image. b–d) Atomic-resolution HAADF image in the surface region, local layered, and spinel-like phases are enlarged from the red and green frames, respectively, as indicated by the overlaid structural models. e–h) Elemental distribution of Co (red), Ti (green), and O (blue) near the surface obtained from electron energy loss spectra mapping. i) Phase constitutions of reaction products of LiCoO₂ and LATP heat-treated at different temperatures. j) Schematic illustration of the surface layer growth mechanism. The spinel phase is structurally more stable than the layered phase with weaker oxygen-anion oxidizing ability at high voltages.

Co₂TiO₄) which are structurally coherent to the layered lattice of LiCoO₂ (Figure 2j). The exclusive formation of the spinel phases enables the growth on the surface of LiCoO₂, ensuring the uniform and conformal coating on particle surface as revealed by the STEM images. From the chemistry point of view, the incorporation of Ti has been demonstrated to be effective on the stabilization of lattice oxygen at high voltages.^[11] In addition, it is known that Li₃PO₄ has appropriate lithium ionic conducting ability and is chemically stable at high voltages, which can promise a high-voltage-stable interface with suitable lithium diffusion kinetics.^[13] It should be noted that while the surface reaction of LATP and LiCoO₂ may not exactly follow the exact reactions as predicted by XRD analysis, it well coincided with the phase evolution trend as revealed, elucidating the key role of the heat annealing process and the critical annealing temperature for the synthesis.

The electronic structure of the LATP@LCO-700 was further studied by soft X-ray absorption spectroscopy (sXAS) to illuminate the valence state of Co via various signal acquisition modes, that is, the total electron yield (TEY) and total fluorescence yield (TFY). Owing to the difference escape depth of secondary electrons and emitted photons, TEY mode has a probing depth of 2–5 nm, while TFY mode probes the bulk signal up to a depth of around 100 nm, respectively.^[14] The Co L-edge sXAS spectra of the bare-LCO and LATP@LCO-700 are shown in Figure S10 in the Supporting Information. While only Co³⁺ feature was found in the bulk signal with TFY, a typical Co²⁺ pre-edge absorption at ≈776 eV was detected by TEY on

the surface of both samples, such feature can be assigned to the spinel species, Co₃O₄ and Co₂TiO₄/CoAl₂O₄.^[15] Noteworthy, the TEY peak intensity at 776 eV for LATP@LCO-700 is larger than that of bare-LCO, it suggests that a larger amount of low valence Co containing spinel species exist on LATP@LCO-700 surface than that of the bare-LCO. Thus, taken together, these findings indicate that the grown ultrathin coating on LATP@LCO-700 can be composed of Co₃O₄, Co₂TiO₄/CoAl₂O₄, and Li₃PO₄, as schematically illustrated in Figure 2j.

The effectiveness of the surface modification in stabilizing LiCoO₂ cathode was evaluated by electrochemical tests in half-cells within 3–4.6 V. Figure 3a,b shows the selected galvanostatic charge/discharge profiles of bare-LCO and LATP@LCO-700 for the 1st and the 50th cycle, which exhibit a high initial discharge capacity of 220.1 and 214.6 mAh g^{−1} at 0.2C, respectively. After 50 cycles, the bare-LCO only remains 151.6 mAh g^{−1}, which is much lower than that of LATP@LCO-700 (200.8 mAh g^{−1}). For the 1st cycle, both cathodes exhibit notable voltage plateaus at ≈3.82, ≈4.2 and ≈4.5 V in the charge/discharge profiles, which can be attributed to the structural transition between two O3 phases, order–disorder transition, and the phase transition between O3 and H1-3 phase, respectively.^[16] After 50 cycles, while the voltage plateau at ≈4.2 V disappears and the voltage plateaus at ≈3.82 and ≈4.5 V become shorter for the bare-LCO sample, those voltage plateaus are remained for the LATP@LCO-700 cathode, indicating a promoted reversibility of the structural transition in the bulk of LiCoO₂ with surface modification.

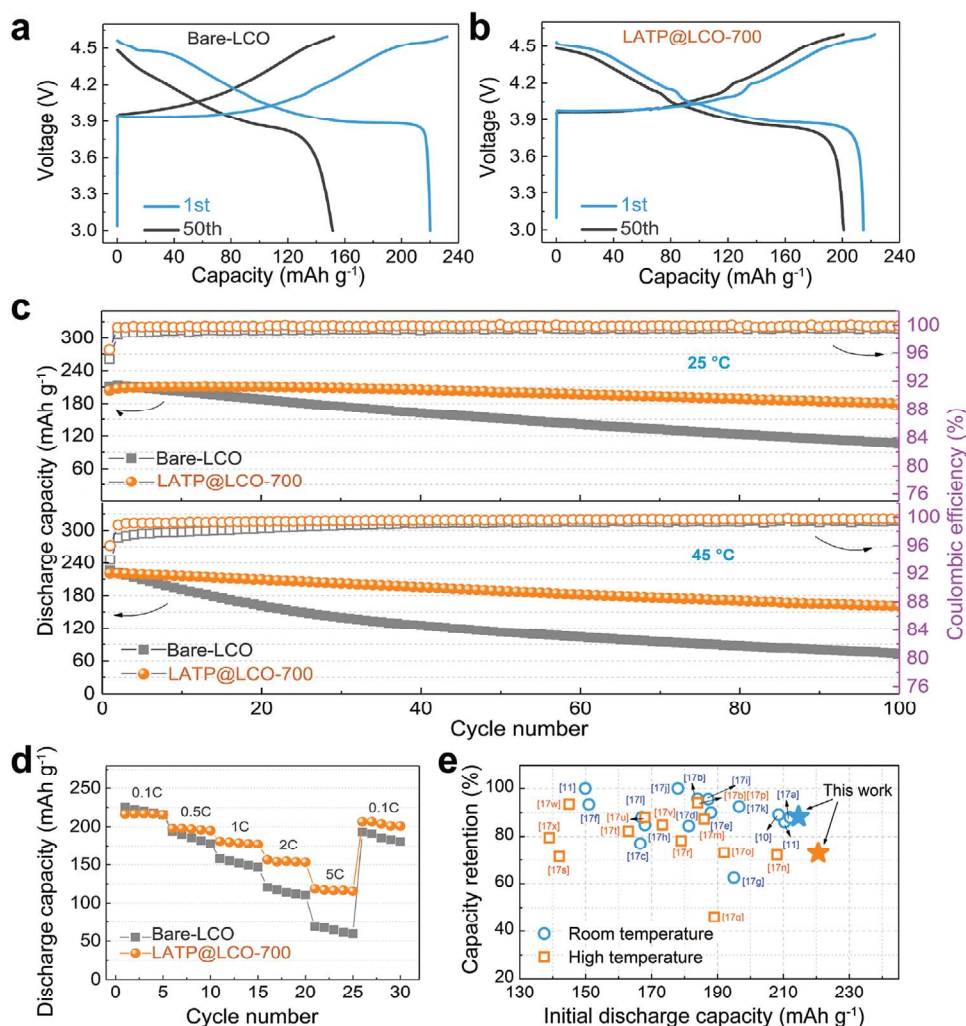


Figure 3. The electrochemical performance of bare-LCO and LATP@LCO-700-based half-cells: charge and discharge curves for a) the 1st cycle at 0.2C and b) the 50th cycle at 0.5C (1C = 274 mA g⁻¹). c) Cycling performance of the cells cycled at 0.5C at various temperatures of 25 and 45 °C. d) Rate performance of the cells at room temperature at 0.1C, 0.5C, 1C, 2C, and 5C. e) Comparison of the cycling retention and initial discharge capacity of various LiCoO₂ materials.

Figure 3c shows the cycle performance of bare-LCO and LATP@LCO-700-based cells under a rate of 0.5C at 25 and 45 °C, respectively. It is found that, when cycled at 25 °C, the bare-LCO cathode can deliver a discharge capacity retention of 50.3% with a capacity of 106 mAh g⁻¹ remains after 100 cycles, while the LATP@LCO-700 exhibits a higher discharge capacity retention of 88.3% with a larger capacity of 180.3 mAh g⁻¹. The LATP@LCO-700 exhibits even superior cycle performances to bare-LCO at 45 °C, with 72.9% of discharge capacity retention (160.9 mAh g⁻¹) versus 32.5% (73.7 mAh g⁻¹) for bare-LCO after 100 cycles. The rate capabilities of the bare-LCO and LATP@LCO-700 are also compared in Figure 3d. While the bare-LCO exhibits discharge capacity of 225.5, 193.7, 157.6, 120.4, and 68.5 mAh g⁻¹ under 0.1C, 0.5C, 1C, 2C, and 5C, respectively, indicating a capacity retention of 30.3% at 5C, the LATP@LCO-700 exhibits discharge capacity of 216.3, 197.8, 181.1, 156.2, and 118.6 mAh g⁻¹ at 0.1C, 0.5C, 1C, 2C, and 5C, respectively, giving a superior capacity retention of 54.8% at 5C. Thus, these results indicate that engineering a surface coating with hybrid phases

for LiCoO₂ can not only enhance the cycle stability of the cathode, but also improve the rate capability. Specifically, the stable spinel phases can stabilize the interface between the cathode and electrolyte, while the Li-ion conductive Li₃PO₄ and LATP phases provide a high ionic transport pathway for facilitating interfacial kinetics, which synergistically contribute to the enhancement of cycle and rate performances of LATP@LCO-700 at harsh condition of high charging voltage and elevated temperature. Moreover, when compared with the results of the previously reported surface-modified LiCoO₂ cathodes, the LATP@LCO-700 also demonstrates a superior performance with the high initial discharge capacity and the excellent capacity retention, and best high-temperature cycle performances among the reported results (Figure 3e; Tables S3 and S4, Supporting Information).^[10,11,17]

To understand how the grown hybrid phase on LCO regulates the interfacial properties and thus enhances the electrochemical performances, electrochemical impedance spectroscopy (EIS) and X-ray spectroscopic characterizations were performed.

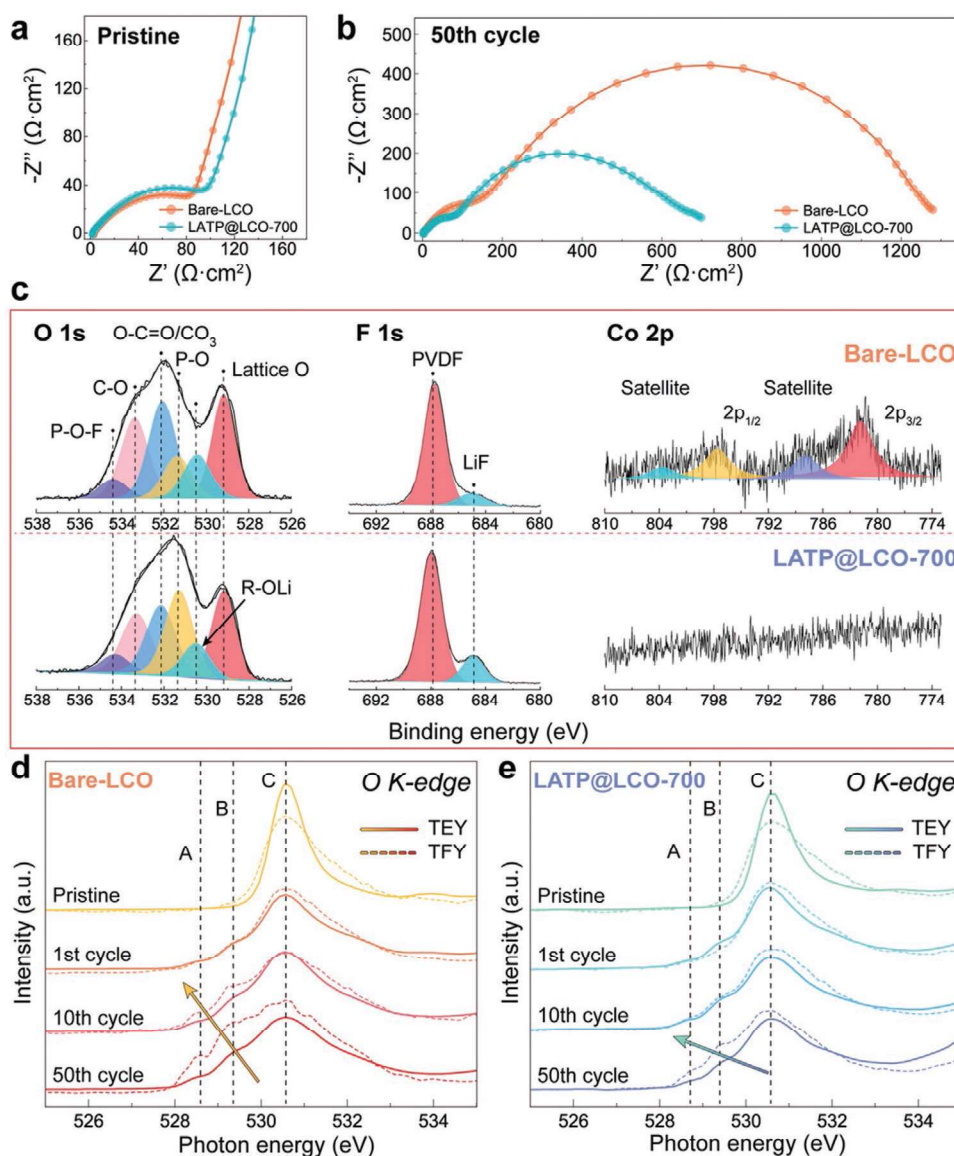


Figure 4. Electrochemical and structural characterization of bare-LCO and LATP@LCO-700 cathode upon cycling. a,b) Electrochemical impedance spectroscopy of the cathode before and after 50 cycles. c) O 1s and F 1s XPS spectra of the cycled cathode, and Co 2p XPS spectra collected on lithium metal anode after 50 cycles. d,e) O K-edge XAS spectra of the bare-LCO and LATP@LCO-700 at various cycling stages.

Figure 4a,b shows the EIS spectra collected for the bare-LCO and the LATP@LCO-700 cells before and after 50 cycles. The quantitative analysis was performed by fitting the spectra with an equivalent circuit model and the fitting results are shown in Figure S11 and Table S5 in the Supporting Information. It can be found that the bare-LCO and the LATP@LCO-700 cells exhibit very similar impedance behavior before cycling. However, after 50 cycles, the bare-LCO cell displays a significantly increased surface film resistance (R_{SEI} , electrode/electrolyte interface) and charge-transfer resistance (R_{ct}) when compared with that of the LATP@LCO-700 cell, suggesting a significantly deteriorated electrode/electrolyte interface.^[18] The improvement on the interfacial stability of the LATP@LCO-700 cell can be attributed to the physical isolation of the electrolyte

from LiCoO_2 by the stable hybrid phase protective coating layer, which could not only mitigate the undesirable interfacial side reactions but also facilitate the Li-ion transportation between the electrolyte and the cathode. XPS experiment was conducted to study the surface chemistry information of CEI on the LiCoO_2 electrode. Figure S12a in the Supporting Information and Figure 4c shows the O 1s and F 1s XPS analysis for the bare-LCO and LATP@LCO-700 electrodes before and after 50 cycles, respectively. It reveals that the CEI formed on the bare-LCO and LATP@LCO-700 electrodes after cycling has similar chemical components which can be mainly classified as organic carbonate species and inorganic species (LiF and $\text{Li}_x\text{F}_y\text{PO}_z$). Further quantitative analysis of the XPS results in Figure S12b in the Supporting Information indicates that the

cycled LATP@LCO-700 has a smaller ratio of the organic CEI components but a larger ratio of LiF inorganic species when compared with the cycled bare-LCO. The organic CEI species can be derived from the electrolyte degradation, such as the ethylene carbonate (EC) ring-opening, which can be triggered by the highly oxidative Co^{4+} as well as the activated lattice oxygen at high voltage.^[19] The relatively low content of organic CEI components indicates the reduced electrode/electrolyte side reactions, validating the suppressed lattice oxygen oxidizing ability of the spinel phase (Co_3O_4 and $\text{Co}_2\text{TiO}_4/\text{CoAl}_2\text{O}_4$) for LATP@LCO-700. Meanwhile, the high content of inorganic components (e.g., LiF and Li_3PO_4) ensures the high chemical stability of the surface layer at high voltages, which is essential for the stable cycling of LiCoO_2 at 4.6 V.^[3] We have also examined the Co deposition on lithium metal anode. As revealed in Figure 4c, the Co 2p XPS signal can be observed for the lithium anode of the bare-LCO cell, while no such signal can be found for that of the LATP@LCO-700 cell, further supporting the formation of a stable surface layer on LATP@LCO-700, which can effectively prevent Co dissolution from the cathode. Furthermore, sXAS measurements were performed in TEY and TFY modes with different probing depth simultaneously. Therefore, both surface and subsurface bulk information can be obtained. Figure 4d,e shows the O K-edge spectra collected on the bare-LCO and LATP@LCO-700 electrodes at discharged state at different cycles. The peaks of A and B can be assigned to $\text{Co}^{4+}(\text{a}_{1g})\text{-O}$ 2p hybridization states and $\text{Co}^{4+}(\text{e}_g)\text{-O}$ 2p hybridization states, respectively, while the C peak corresponds to $\text{Co}^{3+}(\text{e}_g)\text{-O}$ 2p hybridization states.^[20] For both electrodes at pristine state, only C peak is observed, indicating the Co^{3+} in pristine electrode. However, over cycling since the 1st cycle, two new peaks of A and B emerge and progressively enlarge for both electrodes, revealing the accumulation of Co^{4+} on the surface as well as in the bulk. This result can be associated with the deconstruction of LiCoO_2 structure and polarization enhancement at high cut-off voltage upon cycling, which hinders the lithium reinsertion during the discharge process and thus lead to the existence of Co^{4+} . Compared with the bulk TFY signal, the relatively weak Co^{4+} associated feature in TEY can be attributed to inevitable interface reactions against carbonate electrolyte. By comparison of the characteristic peaks (A and B) for both cathodes, it exhibits much more stable and smaller peak intensity for LATP@LCO-700 when compared with those for bare-LCO, suggesting that a much lower amount of Co^{4+} accumulated on the LATP@LCO-700 and relatively modest recovery over long cycles. This is in good agreement with the higher reversibility of lithiation/delithiation behavior for the LATP@LCO-700 cathode, as reflected on the well-maintained charge–discharge profiles after 50 cycles (Figure 3a,b). Besides, the well-resolved and unchanged Ti L-edge XAS spectra (Figure S13, Supporting Information), for both TEY and TFY signals of the LATP@LCO-700, further validates the well-preserved Ti coordinating environment and thus the crystal structure of LiCoO_2 over the cycling process. In summary, the surface modification enables the formation of a high-voltage-stable surface layer on LiCoO_2 , which can protect the surface structure of LiCoO_2 and also suppress the surface side reaction with electrolyte, thereby contributing to the substantially enhanced cycle stability at both room temperature and elevated temperature.

The thermal stability of the cathode is closely related to battery safety, which is another critical issue for LIBs.^[21] Explicitly, the delithiated oxide cathode material is facial to release O_2 at elevated temperatures that may trigger the combustion reactions and lead to the thermal runaway. Here, hard X-ray absorption spectroscopy (hXAS) experiments were carried out to evaluate the thermal stability of both bare and surface-modified LiCoO_2 . The hXAS spectra can be used to quantify the valence state of 3d TM elements and therefore the oxygen release triggered reduction of TM can be recorded during thermal decomposition.^[22] Figure 5a shows the normalized Co K-edge X-ray absorption near edge structure (XANES) spectra for the bare-LCO and LATP@LCO-700 cathode electrodes. The cathode electrodes were retrieved from half-cell at charged state (4.6 V, $\text{Li}_{0.16}\text{CoO}_2$) and then annealed at different temperatures in the range of 25–350 °C. Overall, for both bare-LCO and LATP@LCO-700, the XANES spectra show a continuous shift to low energy side with the annealing temperatures increase from 25 to 350 °C, indicating the reduction of the high valence Co cations ($\text{Co}^{3.84+}$; mixed valence of Co^{3+} and Co^{4+} deduced from the initial charge capacity).^[23] The insets highlight the pre-edge peaks, which also show a continuous shift to low energy side and a slight increase in peak intensities. This can be attributed to the continuous valance change from Co^{4+} to Co^{3+} as well as local distortion such as an increase of Co^{3+} at the tetrahedral site.^[24] To be brief, the oxygen release occurs at delithiated LiCoO_2 and the layered LiCoO_2 phase transfers into Co_3O_4 spinel phase with the increase of the temperature. To more explicitly describe the thermal decomposition process, we plot the half-height-energy of the XANES spectra, a descriptor for the valence state of TM, versus temperature to quantitatively track the Co reduction process (Figure 5b). A notable difference between bare-LCO and LATP@LCO-700 can be observed at temperatures starting from 200 °C where bare-LCO shows lower half-height-energy values than LATP@LCO-700. This suggests the earlier thermal decomposition of bare-LCO and thus the better thermal stability of LATP@LCO-700. In addition, the differential scanning calorimetry (DSC) analysis was performed to evaluate the thermal decomposition behavior of LiCoO_2 in the presence of an electrolyte. As shown in Figure 5c, three exothermic peaks in the DSC curves were observed during the heating process of the charged Li_xCoO_2 cathode with electrolyte. Specifically, the first peak starting near 210 °C in the DSC for the charged bare-LCO can be associated with the decomposition of solvents on the surface of the active cathode materials as a result of the reduction of Li_xCoO_2 ; the second peak at around 240 °C can be due to the electrolyte combustion caused by O_2 released from the Li_xCoO_2 ; while other peaks at higher temperature can be related to the decomposition of the remaining electrolyte from the electrolyte combustion.^[25] Remarkably, the triggering temperature for the first exothermic peak of the DSC is significantly retarded for the LATP@LCO-700 (221 °C), confirming the superior thermal stability of the LATP@LCO-700. Thus, these results demonstrate that the grown hybrid phase coating layer can effectively mitigate the oxygen release from LiCoO_2 and the subsequent reactions with electrolyte at elevated temperature, leading to the improved thermal stability.

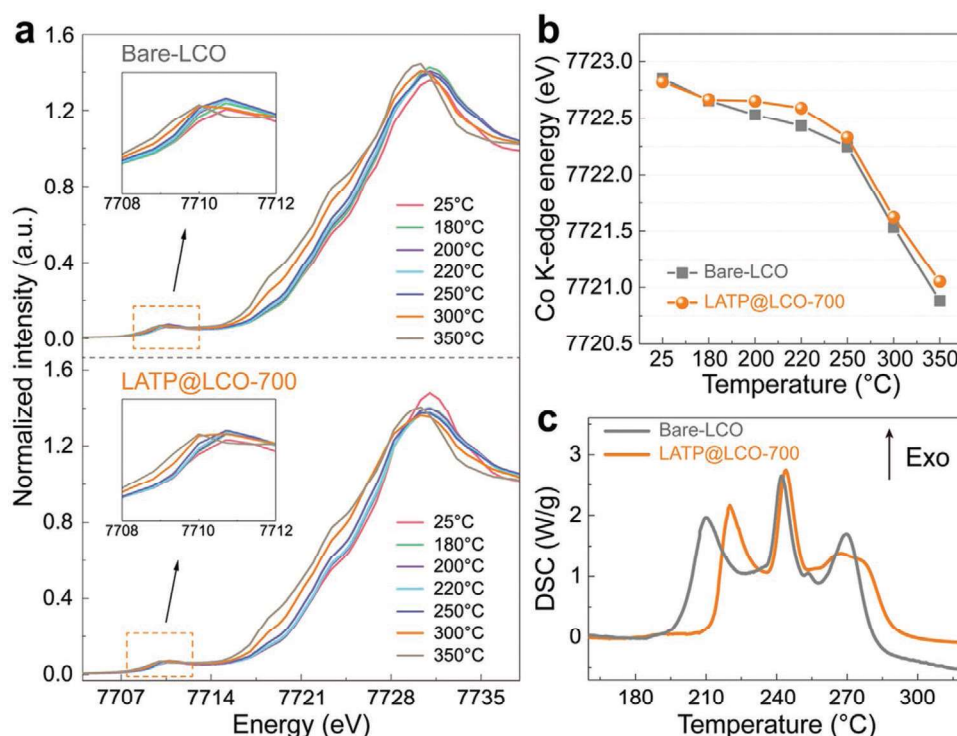


Figure 5. a) Normalized Co K-edge XANES spectra for bare-LCO and LATP@LCO-700 electrodes annealed at various temperatures up to 350 °C after being charged to 4.6 V. b) Variations of the half-energy position of Co K-edge XANES spectra for bare-LCO and LATP@LCO-700 electrodes as a function of annealing temperature. c) Differential scanning calorimetry analysis of bare-LCO and LATP@LCO-700 electrodes wetted with the electrolyte after charging to 4.6 V.

3. Conclusions

In summary, a novel surface modification method has been successfully developed, which demonstrates its effectiveness on the enhancement of the high-voltage cycle and thermal stability of LiCoO₂. We discover that LiCoO₂ can react with LATP at 700 °C to form exclusively the spinel phases (Co₃O₄, CoAl₂O₄, and Co₂TiO₄) in addition to Li₃PO₄, which have coherent lattice structure to layered lattice of LiCoO₂, enabling the formation of a surface coating layer on LiCoO₂. The stable spinel phases can suppress the occurrence of oxygen redox evolution at high voltages and elevated temperatures, and also avoid direct exposure of highly oxidative Co⁴⁺ to electrolyte, effectively mitigating electrolyte degradation and surface structure deconstruction. In addition, the lithium ion conductive phase Li₃PO₄ is not merely high-voltage chemically stable but also provides a facilitated interfacial lithium ion diffusion pathway. Taken all these benefits together, the LiCoO₂ with surface modification through 700 °C heat annealing, the precoated LATP layer exhibits the significantly enhanced discharge capacity retentions of 88.3% and 72.9% at 0.5C for 100 cycles when cycled at room temperature and 45 °C, respectively, which are much higher than those of bare-LCO (only 50.3% and ≈32.5% capacity remains, respectively). Moreover, the XANES and DSC experiments reveal that the thermal stability of the LiCoO₂ has been greatly improved as well. In brief, this work demonstrates an effective surface modification method that enables the formation of a high-quality surface layer for stable cycling of the

LiCoO₂ cathode at high voltages, which could be widely applicable to the designs of other high-voltage and high-energy-density cathode materials.

4. Experimental Section

Synthesis of LiCoO₂ Materials: The bare LiCoO₂ (bare-LCO) powder (with 0.2 wt% Ti doping) employed in this work is commercial. To synthesize the LATP, a mixture of Li₂CO₃, Al₂O₃, TiO₂, and NH₄H₂PO₄ precursors was ground by ball milling at room temperature for 5 h and heated at 400 °C for 2 h followed by 900 °C for 5 h in air. The as-prepared LATP was grounded by a pulverizer to form fine particles with a size of hundreds of nanometers (Figures S1 and S2, Supporting Information), and then 2 wt% of the pulverized LATP was added to LiCoO₂ powder to form a homogenous mixture with a VC blending and modifying machine (VCH-5, Wuxi Xinguang Powder Equipment Co., Ltd., China). The mixture was then further mechanically mixed at 3000 rpm min⁻¹ for 20 min using a mechanical fusion device (VSH-3, Wuxi Xinguang Powder Equipment Co., Ltd., China), which can perform uniform particle coating for industrial level fabrication. Last, the mixture was calcined in air at 400, 550, 700, 800, and 900 °C for 4 h, respectively, to obtain various LATP modified-LiCoO₂ samples.

Electrochemical Measurements: The positive electrodes were fabricated with 92 wt% active material, 3 wt% carbon black as a conductive additive, and 5 wt% polytetrafluoroethylene as a binder. The calculated amount of powder was dissolved in *N*-methyl pyrrolidone solvent to obtain a homogeneous slurry, which was then cast onto aluminum foil with a blade and dried at 120 °C in vacuum for 6 h. Then, the electrodes were cut into disks (Φ10 mm, with 3 mg cm⁻² active material). Coin cells (CR 2032) were assembled with bare-LCO or various LATP modified LiCoO₂

materials as cathode materials, lithium foil as the anode, polypropylene as separators, and 1 M LiPF₆ in ethylene carbonate/dimethyl carbonate (EC/DMC, 1:1 in volume) as an electrolyte in an argon-filled glovebox. The galvanostatic charge–discharge tests were carried out in the voltage range of 3.0–4.6 V using a Land CT2001A battery test system (Land, Wuhan, China). The EIS was measured at 25 °C by an impedance analyzer (IM6ex) with a perturbation of 5 mV in the frequency range 10 mHz to 1 MHz.

SEM, XPS, and XRD Characterization: Morphological investigation and EDS mapping analysis of the samples were conducted using a field emission scanning electron microscope with an energy dispersive X-ray detector (SEM, S4800, Hitachi). The crystal structure of samples was analyzed by XRD (Bruker, D8 ADVANCE). The XPS spectra were recorded by an ESCALAB 250 Xi, Thermo Fisher with monochromatic 150 W Al K α radiation. The XPS data were analyzed with software Avantage and the binding energies were calibrated by the C 1s line at 284.4 eV from carbon black. In order to avoid the air exposure, all XPS samples after cycling were transferred with an air-proof sample holder provided by Thermo Fisher.

STEM Characterization: TEM sample was prepared using a focused ion beam (FIB) method. Cross-sectional lamella was thinned down to 100 nm thick at an accelerating voltage of 30 kV with a decreasing current from the maximum 2.5 nA, followed by fine polish at an accelerating voltage of 2 kV with a small current of 40 pA. The atomic structure of the LiCoO₂ was characterized using an ARM-200CF (JEOL, Tokyo, Japan) transmission electron microscope operated at 200 keV and equipped with double spherical aberration (Cs) correctors. The attainable resolution of the probe defined by the objective prefield was 78 pm. The HAADF images were acquired with a collection angle of 90–370 mrad. The EELS elemental mapping was performed with an energy dispersion of 1 eV per channel.

X-Ray Absorption Spectra (XAS) Characterization: The soft-XAS measurements were recorded at beamline 8.0.1 of the Advanced Light Source (ALS) at Lawrence Berkeley National Laboratory. The data were collected in both TEY and TFY modes. All the spectra were normalized by the intensity of the incident beam. The hard-XAS data were collected at beamline BL14W at Shanghai Synchrotron Radiation Facility (SSRF). XANES spectra were processed using the Athena software. The electrodes after the first charge were heated for 15 min at different temperatures in the muffle furnace placed in the glovebox.

Thermogravimetric-Differential Scanning Calorimetry (TG-DSC) Characterization: The TG-DSC analysis was carried out using a simultaneous thermal analyzer (Netzsch STA 449 C) with a heating rate of 5 °C min^{−1} in air. The samples for TG-DSC analysis were prepared with 4 mg cathode materials and 10 μ L electrolyte loading into a stainless-steel pan sealed with a gold-plated copper seal.

Supporting Information

Supporting Information is available from the Wiley Online Library or from the author.

Acknowledgements

Y.W., Q.Z., and Z.X. contributed equally to this work. The work was supported by funding from the National Key R&D Program of China (2016YFB0100100), the National Natural Science Foundation of China (grant nos. 51822211 and U1932220), and the Foundation for Innovative Research Groups of the National Natural Science Foundation of China (grant no. 51421002). Soft X-ray spectroscopic experiments used resources of the Advanced Light Source, which is a U.S. Department of Energy Office of Science User Facility under contract no. DE-AC02-05CH11231. The authors gratefully acknowledge the technical help from beamline BL14W1 at Shanghai Synchrotron Radiation Facility (SSRF, China).

Conflict of Interest

The authors declare no conflict of interest.

Keywords

cathodes, lithium cobalt oxide, lithium-ion batteries, solid electrolytes, surface coating

Received: April 24, 2020

Revised: May 21, 2020

Published online: June 15, 2020

- [1] a) K. Mizushima, P. C. Jones, P. J. Wiseman, J. B. Goodenough, *Mater. Res. Bull.* **1980**, *15*, 783; b) J. B. Goodenough, *Acc. Chem. Res.* **2013**, *46*, 1053.
- [2] a) L. Wang, B. Chen, J. Ma, G. Cui, L. Chen, *Chem. Soc. Rev.* **2018**, *47*, 6505; b) J. Zheng, S. Myeong, W. Cho, P. Yan, J. Xiao, C. Wang, J. Cho, J. G. Zhang, *Adv. Energy Mater.* **2017**, *7*, 1601284.
- [3] Z. Chen, J. R. Dahn, *Electrochim. Acta* **2004**, *49*, 1079.
- [4] a) W. Cho, S. Myeong, N. Kim, S. Lee, Y. Kim, M. Kim, S. J. Kang, N. Park, P. Oh, J. Cho, *Adv. Mater.* **2017**, *29*, 1605578; b) M. D. Radin, S. Hy, M. Sina, C. Fang, H. Liu, J. Vinckeviciute, M. Zhang, M. S. Whittingham, Y. S. Meng, A. Van der Ven, *Adv. Energy Mater.* **2017**, *7*, 1602888.
- [5] a) A. Yano, M. Shikano, A. Ueda, H. Sakaebe, Z. Ogumi, *J. Electrochem. Soc.* **2017**, *164*, A6116; b) Y. Xu, E. Hu, K. Zhang, X. Wang, V. Borzenets, Z. Sun, P. Pianetta, X. Yu, Y. Liu, X.-Q. Yang, H. Li, *ACS Energy Lett.* **2017**, *2*, 1240; c) C. Qin, Y. Jiang, P. Yan, M. Sui, *J. Power Sources* **2020**, *460*, 228126; d) A. M. Nolan, Y. Liu, Y. Mo, *ACS Energy Lett.* **2019**, *4*, 2444.
- [6] a) D. Enslin, G. Cherkashinin, S. Schmid, S. Bhuvanawari, A. Thissen, W. Jaegermann, *Chem. Mater.* **2014**, *26*, 3948; b) J. B. Goodenough, Y. Kim, *Chem. Mater.* **2010**, *22*, 587; c) K. Luo, M. R. Roberts, R. Hao, N. Guerrini, D. M. Pickup, Y. S. Liu, K. Edstrom, J. Guo, A. V. Chadwick, L. C. Duda, P. G. Bruce, *Nat. Chem.* **2016**, *8*, 684; d) K. Nie, X. Wang, J. Qiu, Y. Wang, Q. Yang, J. Xu, X. Yu, H. Li, X. Huang, L. Chen, *ACS Energy Lett.* **2020**, *5*, 826.
- [7] a) J.-N. Zhang, Q. Li, Y. Wang, J. Zheng, X. Yu, H. Li, *Energy Storage Mater.* **2018**, *14*, 1; b) Q. Li, Y. Wang, X. Wang, X. Sun, J. N. Zhang, X. Yu, H. Li, *ACS Appl. Mater. Interfaces* **2020**, *12*, 2319.
- [8] a) S. Kalluri, M. Yoon, M. Jo, H. K. Liu, S. X. Dou, J. Cho, Z. Guo, *Adv. Mater.* **2017**, *29*, 1605807; b) S. Kalluri, M. Yoon, M. Jo, S. Park, S. Myeong, J. Kim, S. X. Dou, Z. Guo, J. Cho, *Adv. Energy Mater.* **2017**, *7*, 1601507.
- [9] a) H. Li, Z. Wang, L. Chen, X. Huang, *Adv. Mater.* **2009**, *21*, 4593; b) J.-I. Lee, E.-H. Lee, J.-H. Park, S. Park, S.-Y. Lee, *Adv. Energy Mater.* **2014**, *4*, 1301542; c) C.-W. Wang, Y. Zhou, J.-H. You, J.-D. Chen, Z. Zhang, S.-J. Zhang, C.-G. Shi, W.-D. Zhang, M.-H. Zou, Y. Yu, J.-T. Li, L.-Y. Zeng, L. Huang, S.-G. Sun, *ACS Appl. Energy Mater.* **2020**, *3*, 2593; d) J. Xie, J. Zhao, Y. Liu, H. Wang, C. Liu, T. Wu, P.-C. Hsu, D. Lin, Y. Jin, Y. Cui, *Nano Res.* **2017**, *10*, 3754; e) A. Zhou, Q. Liu, Y. Wang, W. Wang, X. Yao, W. Hu, L. Zhang, X. Yu, J. Li, H. Li, *J. Mater. Chem. A* **2017**, *5*, 24361; f) Q. Yang, J. Huang, Y. Li, Y. Wang, J. Qiu, J. Zhang, H. Yu, X. Yu, H. Li, L. Chen, *J. Power Sources* **2018**, *388*, 65; g) Z. Wang, Z. Wang, H. Guo, W. Peng, X. Li, G. Yan, J. Wang, *J. Alloys Compd.* **2015**, *621*, 212; h) S. Sharifi-Asl, F. A. Soto, T. Foroozan, M. Asadi, Y. Yuan, R. Deivanayagam, R. Rojaee, B. Song, X. Bi, K. Amine, *Adv. Energy Mater.* **2019**, *29*, 1901110; i) Q. Liu, X. Su, D. Lei, Y. Qin, J. Wen, F. Guo, Y. A. Wu, Y. Rong, R. Kou, X. Xiao, F. Aguesse, J. Bareno, Y. Ren, W. Lu, Y. Li, *Nat. Energy* **2018**, *3*, 936.

- [10] J. Qian, L. Liu, J. Yang, S. Li, X. Wang, H. L. Zhuang, Y. Lu, *Nat. Commun.* **2018**, 9, 4918.
- [11] J.-N. Zhang, Q. Li, C. Ouyang, X. Yu, M. Ge, X. Huang, E. Hu, C. Ma, S. Li, R. Xiao, W. Yang, Y. Chu, Y. Liu, H. Yu, X.-Q. Yang, X. Huang, L. Chen, H. Li, *Nat. Energy* **2019**, 4, 594.
- [12] a) D. S. Hall, R. Gauthier, A. Eldesoky, V. S. Murray, J. R. Dahn, *ACS Appl. Mater. Interfaces* **2019**, 11, 14095; b) Y. Orikasa, D. Takamatsu, K. Yamamoto, Y. Koyama, S. Mori, T. Masese, T. Mori, T. Minato, H. Tanida, T. Uruga, Z. Ogumi, Y. Uchimoto, *Adv. Mater. Interfaces* **2014**, 1, 1400195; c) Y.-K. Sun, C. S. Yoon, S.-T. Myung, I. Belharouak, K. Amine, *J. Electrochem. Soc.* **2009**, 156, A1005; d) B. Hu, X. Lou, C. Li, F. Geng, C. Zhao, J. Wang, M. Shen, B. Hu, *J. Power Sources* **2019**, 438, 226954.
- [13] A. T. Appapillai, A. N. Mansour, J. Cho, Y. Shao-Horn, *Chem. Mater.* **2007**, 19, 5748.
- [14] W. Yang, X. Liu, R. Qiao, P. Olalde-Velasco, J. D. Spear, L. Roseguo, J. X. Pepper, J. D. Denlinger, Z. Hussain, *J. Electron Spectrosc. Relat. Phenom.* **2013**, 190, 64.
- [15] D. K. Bora, X. Cheng, M. Kapilashrami, P. A. Glans, Y. Luo, J. H. Guo, *J. Synchrotron Radiat.* **2015**, 22, 1450.
- [16] a) J. N. Reimers, J. R. Dahn, *J. Electrochem. Soc.* **1992**, 139, 2091; b) A. Van der Ven, M. Aydinol, G. Ceder, G. Kresse, J. Hafner, *Phys. Rev. B* **1998**, 58, 2975; c) C. A. Marianetti, G. Kotliar, G. Ceder, *Nat. Mater.* **2004**, 3, 627.
- [17] a) L. Wang, J. Ma, C. Wang, X. Yu, R. Liu, F. Jiang, X. Sun, A. Du, X. Zhou, G. Cui, *Adv. Sci.* **2019**, 6, 1900355; b) N. Xu, H. Zhou, Y. Liao, G. Li, M. Xu, W. Li, *Solid State Ionics* **2019**, 341, 115049; c) F. Chen, Y. Liao, M. Li, J. Huang, Q. Huang, W. Li, *J. Electrochem. Soc.* **2018**, 165, A206; d) A. Zhou, W. Wang, Q. Liu, Y. Wang, X. Yao, F. Qing, E. Li, T. Yang, L. Zhang, J. Li, *J. Power Sources* **2017**, 362, 131; e) A. Zhou, X. Dai, Y. Lu, Q. Wang, M. Fu, J. Li, *ACS Appl. Mater. Interfaces* **2016**, 8, 34123; f) S. Sheng, G. Chen, B. Hu, R. Yang, Y. Xu, *J. Electroanal. Chem.* **2017**, 795, 59; g) M. Xie, T. Hu, L. Yang, Y. Zhou, *RSC Adv.* **2016**, 6, 63250; h) L. Xia, Y. Xia, Z. Liu, *Electrochim. Acta* **2015**, 151, 429; i) Y. Ji, S. Li, G. Zhong, Z. Zhang, Y. Li, M. J. McDonald, Y. Yang, *J. Electrochem. Soc.* **2015**, 162, A7015; j) Z. Chen, J. R. Dahn, *Electrochem. Solid-State Lett.* **2003**, 6, A221; k) X. Kong, R. Zhou, J. Wang, J. Zhao, *ACS Appl. Energy Mater.* **2019**, 2, 4683; l) J.-M. Chen, Y.-D. Cho, C.-L. Hsiao, G. T.-K. Fey, *J. Power Sources* **2009**, 189, 279; m) M. Zhang, J. Zhang, J. Yang, X. Du, Z. Chen, K. Chen, C. Lu, H. Zhang, T. Dong, J. Li, Z. Zhang, H. Zhang, G. Cui, *J. Electrochem. Soc.* **2019**, 166, A2313; n) L. Shao, L. Zhou, L. Yang, C. Jia, C. Wang, S. Hu, X. Zeng, C. Yang, C. Huang, Y. Zhou, X. Xi, *Electrochim. Acta* **2019**, 297, 742; o) J. Lim, A. Choi, H. Kim, S. W. Doo, Y. Park, K. T. Lee, *J. Power Sources* **2019**, 426, 162; p) R. Gu, T. Cheng, Z. Ma, R. Qian, Y. Lyu, A. Nie, B. Guo, *J. Alloys Compd.* **2019**, 803, 348; q) A. Zhou, Y. Lu, Q. Wang, J. Xu, W. Wang, X. Dai, J. Li, *J. Power Sources* **2017**, 346, 24; r) A. Zhou, J. Xu, X. Dai, B. Yang, Y. Lu, L. Wang, C. Fan, J. Li, *J. Power Sources* **2016**, 322, 10; s) J. Zhang, R. Gao, L. Sun, H. Zhang, Z. Hu, X. Liu, *Electrochim. Acta* **2016**, 209, 102; t) N. Wu, Y. Zhang, Y. Wei, H. Liu, H. Wu, *ACS Appl. Mater. Interfaces* **2016**, 8, 25361; u) N. Wu, Y. Zhang, Y. Guo, S. Liu, H. Liu, H. Wu, *ACS Appl. Mater. Interfaces* **2016**, 8, 2723; v) P. Qi, Y. Han, J. Zhou, X. Fu, S. Li, J. Zhao, L. Wang, X. Fan, X. Feng, B. Wang, *Chem. Commun.* **2015**, 51, 12391; w) L. Zhang, Y. Sun, Y. Zhou, C. Hai, S. Hu, J. Zeng, Y. Shen, S. Dong, G. Qi, F. Li, *Ionics* **2018**, 24, 2995; x) S. Byun, J. Choi, Y. Roh, D. Song, M.-H. Ryou, Y. M. Lee, *Electrochim. Acta* **2020**, 332, 135471.
- [18] R. Gu, Z. Ma, T. Cheng, Y. Lyu, A. Nie, B. Guo, *ACS Appl. Mater. Interfaces* **2018**, 10, 31271.
- [19] M. Gauthier, P. Karayalali, L. Giordano, S. Feng, S. F. Lux, F. Maglia, P. Lamp, Y. Shao-Horn, *J. Electrochem. Soc.* **2018**, 165, A1377.
- [20] T. Mizokawa, Y. Wakisaka, T. Sudayama, C. Iwai, K. Miyoshi, J. Takeuchi, H. Wadati, D. G. Hawthorn, T. Z. Regier, G. A. Sawatzky, *Phys. Rev. Lett.* **2013**, 111, 056404.
- [21] R. Chen, Q. Li, X. Yu, L. Chen, H. Li, *Chem. Rev.* **2019**, <https://doi.org/10.1021/acs.chemrev.9b00268>.
- [22] D. Takamatsu, Y. Koyama, Y. Orikasa, S. Mori, T. Nakatsutsumi, T. Hirano, H. Tanida, H. Arai, Y. Uchimoto, Z. Ogumi, *Angew. Chem., Int. Ed.* **2012**, 51, 11597.
- [23] Y. Lee, M. G. Kim, J. Kim, Y. Kim, J. Cho, *J. Electrochem. Soc.* **2005**, 152, A1824.
- [24] K.-W. Nam, S.-M. Bak, E. Hu, X. Yu, Y. Zhou, X. Wang, L. Wu, Y. Zhu, K.-Y. Chung, X.-Q. Yang, *Adv. Funct. Mater.* **2013**, 23, 1047.
- [25] a) S. H. Lee, J.-M. Jung, J. H. Ok, C.-H. Park, *J. Power Sources* **2010**, 195, 5049; b) J.-I. Yamaki, Y. Baba, N. Katayama, H. Takatsuji, M. Egashira, S. Okada, *J. Power Sources* **2003**, 119–121, 789.